Petra Mela[1, 3]
Albert van den Berg[1]
Yolanda Fintschenko[3]
Eric B. Cummings[3]
Blake A. Simmons[2]
Brian J. Kirby[3]

[1]BIOS, MESA$^+$ Institute for
 Nanotechnology,
 University of Twente,
 The Netherlands
[2]Materials Chemistry Department,
 Sandia National Laboratories,
 Livermore, CA, USA
[3]Microfluidics Department,
 Sandia National Laboratories,
 Livermore, CA, USA

The zeta potential of cyclo-olefin polymer microchannels and its effects on insulative (electrodeless) dielectrophoresis particle trapping devices

While cyclo-olefin polymer microchannels have the potential to improve both the optical detection sensitivity and the chemical resistance of polymer microanalytical systems, their surface properties are to date not thoroughly characterized. These surface properties dictate, among other things, electrokinetic effects when electric fields are present. Here, we report the measurement of the zeta potential of cyclo-olefin polymers (injection-molded and hot-embossed Zeonor® 1060R and 1020R) microchannels as a function of pH, counter-ion concentration, storage conditions, and chemical treatment in aqueous solutions both with and without EOF-suppressing additives. In contrast with previous reports, significant surface charge is measured, consistent with titration of charged sites with pK_a = 4.8. Storage in air, acetonitrile, or aqueous solutions has relatively minor effects. While the source of the surface charge is unclear, chemical functionalization has shown that carboxylic acid groups are not present at the surface, consistent with the chemical structure of Zeonor®. EOF-suppressing additives (hydroxypropylmethylcellulose) and conditioning in perchloric acid allow the surface charge to be suppressed. We demonstrate dielectrophoretic particle trapping devices in Zeonor® 1060R substrates that show reduced trapping voltage thresholds as compared to previous implementations in glass.

1 Introduction

The increasing interest in micrototal analysis system (µTAS) applications in the past decade has led to the introduction of new techniques and materials. Polymers have received increasing attention in the µTAS community as promising substrates for mass replication technologies, such as injection molding and hot embossing, as well as rapid prototyping techniques, such as casting and laser micromachining. A wide variety of polymer materials has been used for microfabrication processes [1]. To date, poly(methylmethacrylate) (PMMA) and polycarbonate (PC) are the most popular polymer materials for microfabrication *via* hot embossing and injection molding [2–6]. Much of the work on electrokinetic potentials observed on plastic substrates is summarized in [7]. Recently, cyclo-olefin polymers and copolymers have also received attention because of their high chemical stability and optical transparency, which make them promising materials for applications in analytical chemistry, chemical engineering, and molecular biotechnology. Zeonor® resins, for example, are cyclo-olefin polymers that exhibit low water absorbency, high transparency, and good chemical resistance, making them well-suited for difficult microchip design problems that include organic solvents and optical detection.

Implementing microanalytical systems for capillary electrophoresis separations requires an understanding of the electroosmotic mobility of the system, which is closely related to the surface zeta potential of the substrate. Unfortunately, the zeta potential of cyclo-olefin resins is not well-characterized. Previously reported experiments [8] with aqueous liquids in hot-embossed Zeonor® 1020R

microchannels indicated that the electroosmotic mobility was immeasurably small unless the polymer surface was plasma-oxidized, and work in Zeonor® [9, 10] has paid relatively little attention to the magnitude of the electrokinetic potential. Evidence in our laboratory with electric field manipulation of cell suspensions in hot-embossed and injection-molded cyclo-olefin polymer microchips has indicated that the microchannels show measurable electroosmotic mobility, often in excess of the electrophoretic mobility of cells or latex particles. Here, we report a systematic study of the zeta potential of microfluidic channels fabricated by injection molding and hot embossing of two different Zeonor® resins. The dependence of zeta on buffer pH, counterion concentration, storage, chemical treatment, and EOF-suppressing additives are shown. We also report implementation of a Zeonor® 1060R electrodeless dielectrophoresis device for trapping particles and observe the effects of these Zeta potentials on trapping threshold voltages.

2 Materials and methods

2.1 Chemical reagents and solutions

All reagents were obtained from Sigma-Aldrich (St. Louis, MO, USA) unless specified otherwise. Phosphate buffers were prepared from stock solutions of monobasic and dibasic potassium phosphate except at pH 1.8 at which 10 mM phosphoric acid was used. Acetate buffers were prepared from sodium acetate and glacial acetic acid; Tris buffers were prepared by titrating Tris base with HCl. Borate buffers were prepared with sodium borate in deionized water. Solution conductivity and pH were measured with a conductivity meter (Corning 441; Corning, NY, USA) and a pH meter (model 250; Denver Instrument, Denver, CO, USA). Fluid viscosity was measured by monitoring the pressure drop of known laminar flow rates through microchannels of known fluidic resistance. 1-Ethyl-3-(3-dimethylaminopropyl) carbodiimide hydrochloride (EDAC) and 5-(aminoacetamido) fluorescein (amino-fluorescein) were obtained from Molecular Probes, (Eugene, OR, USA). A solution of 0.5 mM EDAC and 0.5 mM amino-fluorescein was prepared in 100 mM, pH 7, phosphate buffer.

2.2 Polymer wafer design and fabrication

Polymer wafers were fabricated using injection molding and hot embossing onto nickel stamps electroplated onto micromachined silicon using techniques described below. Six microchannels were fabricated on each wafer; each channel consisted of a serpentine channel nominally 160 μm wide by 70 μm deep by 32 cm long.

2.3 Silicon stamp fabrication

A 1 μm thick layer of OCG 825 positive photoresist (Arch Chemicals, Columbus, OH, USA) was spin-coated and soft-baked onto a 3 mm thick silicon wafer (International Wafer Service, Portola Valley, CA, USA). A Karl Süss MA6 contact mask aligner (Karl Süss America, Waterbury Center, VA, USA) was used to photolithographically define the microchannels using chrome-on-glass masks (Photosciences, San José, CA, USA). After exposure, the photoresist was developed with OCG 934 developer (Arch Chemicals). A cyclical etch-passivation Bosch process was performed in an Oxford Plasmalab 100 ICP system (Oxford Instruments, Concord, MA, USA) using a SF_6 plasma for etching and a C_4F_8 plasma for passivation. Etch depths were measured with a Dektak[3] ST profilometer (Veeco Instruments, Plainview, NY, USA).

2.4 Nickel stamp electroplating

Following etching, the silicon (Si) substrates were coated with 500 Å Ti (adhesion promoter) and 1500 Å Cu (electroplating seed) layers through serial sputter deposition steps. Electroplating (Digital Matrix© Electroforming Machine, model SA/3m; Hempstead, NY, USA) was conducted at 38°C in a traditional nickel (Ni) sulfamate bath [11] at 1 A for 40 h (40 A·h) producing a Ni layer of approximately 950 μm total thickness that contains the opposite tones of the silicon substrates. The Ni stamp was then released from the silicon substrate using traditional wet chemistry techniques (HF bath to remove the Si; NH_4OH bath to remove the metallized layers and expose a clean Ni surface; verification by optical and electron microscopy). The Ni stamps were then machined (2.1 cm outer diameter, 0.076 cm thick) to the appropriate dimensions for use in the injection molding and hot embossing processes using fixtures developed in-house.

2.5 Polymer replication/device formation and storage

A Nissei® (TH-60 Injection Molding Machine, Los Angeles, CA, USA) 60-ton vertical platen device was used for injection molding. The cyclo-olefin polymer thermoplastic resins, Zeonor® 1060R and 1020R, were obtained from Zeon Chemicals (Louisville, KY, USA) and used as received in either pelleted or sheet form. Pelleted thermoplastic resin was fed to the injection molding machine after drying at 60°C for 4 h. Temperature control, process conditions, and cycle times were empirically determined for the resin based on manufacturer's recommendations (www.zeonchemicals.com). Hot embossing was carried out using a Carver© press Carver© Press model 12–12H;

Miniaturization

Wabash, IN, USA) with preformed sheet discs under empirically determined optimal conditions (3400 kg load, 10 min at 125°C; cooled under loading). Lids were fabricated by precision drilling 1 mm diameter holes through a blank polymer disc to match the microchannels. Devices were then sealed with lids through thermal diffusion bonding (96°C, 2300 kg load, 20 min) in a Carver© Press (Carver© Press model 12–12H). The chips were cleaned with acetone and dried with pressurized nitrogen. Experiments were performed within one week of fabrication, except when specified otherwise. To determine the influence of storage conditions, channels were stored in a variety of environments, including air, acetonitrile, and aqueous solutions of varying pH. Channels were stored for a minimum of 10 days at different conditions including: 10 mM phosphate buffers with pH 1.9, 6.9, and 8.8, acetonitrile (ACN), and air. In separate experiments, channels were flushed with a 1% perchloric acid solution for 30 min. In all cases, the channels were flushed thoroughly with 10 mM pH 6.9, phosphate buffer and tested at that condition.

2.6 Fluorescent surface characterization

Zeonor surfaces were incubated with the EDAC/amino-fluorescein solution for 24 h using procedures described in [3]. Fluorescence from covalently attached amino-fluorescein was observed with a microscope.

2.7 Zeta potential measurement

Streaming potential was used to measure the zeta potential in polymer microchannels. Pressure (0–0.6 MPa) was applied to the inlet of the microchannel using a syringe pump. Solutions were flushed through the system for 10 min before data were recorded. Fluidic connections to the microchips were made using 360 μm stainless steel tubing and PEEK-ULTEM fittings [12]. Platinized platinum electrodes connected to a 10 GΩ electrometer (614 Electrometer, Kiethley, Cleveland, OH, USA) measured the generated voltage across the channel and a strain-gauge type transducer (Senso-Metrics SP70D, Simi Valley, CA, USA) measured the pressure at the inlet. The pressure drop measured across the microchip for known flow rates was used to calculate the microchip fluidic resistance, and small (~3–10%) corrections to the measured pressure were made to account for pressure drop across the tubing connecting the pressure transducer to the microchip. The forcing pressure and channel dimensions were chosen such that the flow was laminar, surface conductivity was negligible, and errors due to hydrodynamic starting lengths could be ignored. The zeta potential was calculated using the Smoluchowski equation [13]:

$$\zeta = \frac{\mu \sigma}{\varepsilon \varepsilon_0} \frac{\Delta V}{\Delta P} \qquad (1)$$

where ζ is the electrokinetic or zeta potential, μ is the bulk viscosity, σ is the bulk fluid conductivity, ε is the fluid dielectric constant, ε_0 is the permittivity of free space, and $\Delta V/\Delta P$ is the voltage-pressure slope. As written here, Eq. (1) tacitly assumes that double layers may be assumed thin, that wall curvature may be ignored, and that the Debye-Hückel approximation for the charge distribution in the double layer is suitable for modeling the net convective charge fluxes. The microchannel cross-section in the microchips used here is roughly rectangular. Errors introduced by the wall curvature and the use of
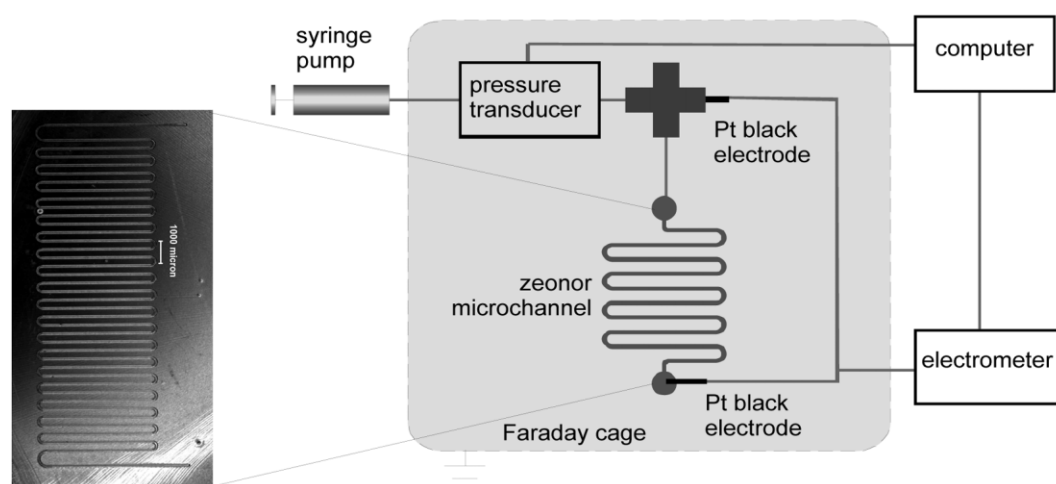

Figure 1. Right: schematic representation of the zeta potential measurement apparatus. Left: optical microscope image of a microchannel.

Eq. (1) to describe non-Debye-Hückel charge distributions are ignored here since they are small as compared to temperature and conductivity uncertainties. Experiments were repeated several times and applied to a number of individual microchannels; the number of measurements (n_m) and number of channels (n_c) used for each datum are specified in Section 3.

2.8 Dielectrophoretic trapping

Optical observation of particle behavior was conducted on an inverted epifluorescence microscope (Olympus IX-71; Napa, CA, USA). Fluorescently labeled (carboxylate-modified, green fluorescent) polystyrene beads were obtained from Molecular Probes (Eugene, OR, USA) and used as received, diluted in deionized water adjusted to pH 8 by titration with NaOH (resulting bulk conductivity = 2.8 µS/cm; particle EP mobility = −1 µm cm/V·s). A flow manifold, developed in-house, was used to control electrode placement and sample delivery. Direct current (DC) electric fields were applied using an high-voltage (HV) power supply (Stanford Research Systems, PS350; Palo Alto, CA, USA). Videos were captured by a digital camera (Sony, San Diego, CA, USA).

3 Results and discussion

3.1 Standards

Before working with microchips, the reliability and accuracy of the setup was tested by measuring the ζ of silica capillaries (Polymicro Technologies, Phoenix, AZ, USA) connected using identical fittings. Capillaries were tested both as received and after coating with polyacrylamide [13]. The measurements were repeated at different stages of the study and the results were consistent. At 10 mM phosphate, pH 7, the zeta potential of bare capillaries was measured as −52 mV (consistent with results summarized in Fig. 6 of [14]). Polyacrylamide-coated capillaries resulted in zeta potential magnitudes that were lower by at least an order of magnitude, consistent with the results in [13].

3.2 Counterion concentration

Measurements of zeta potential of injection-molded Zeonor® 1060R at varying buffer concentrations show the combined effects of double layer shielding and, if present, adsorption (Fig. 2). While the pH 7 zeta potential data plotted *vs.* pC (pC $\equiv$ –log C, where C is the counterion concentration in mol/L) shows some curvature, a linear fit within the range C = 0.5–50 mM matches the data well (r^2 = 0.99) and gives dζ/dlogC = 9.97 mV. Using the
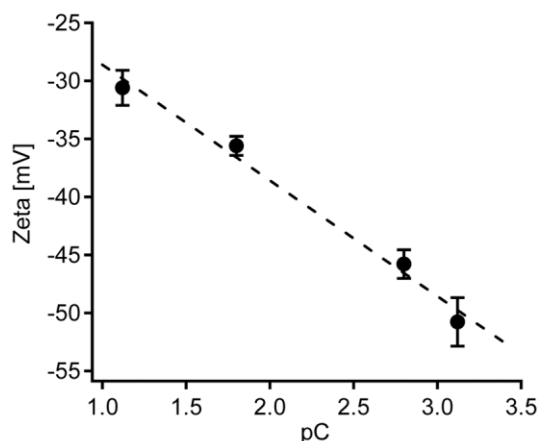
Figure 2. Zeta potential (mean ± SD, n_m = 9, n_c = 3) as a function of the negative logarithm of the counterion concentration (*pC*) of phosphate buffers at pH 6.8–7.0, *C* = 0.5–50 mM. Dashed line: linear fit.
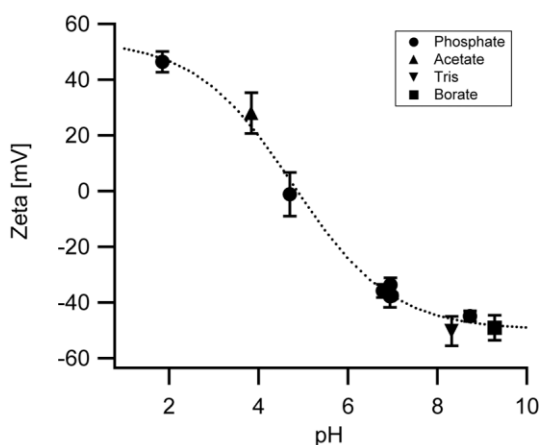

Figure 3. Zeta potential (mean ± SD; n_m = 15, n_c = 5) as a function of buffer pH. The dotted line represents a sigmoidal fit of the experimental points, indicative of titration of charged sites with pK_a near 4.8. Counterion concentration, 10 mM.

dζ/dlogC ζ values obtained at different concentrations can be converted into, for example, equivalent values at 10 mM. Such an approach is particularly helpful to compare data taken at different concentrations.

3.3 pH and buffer type

Streaming potential measurements with a variety of buffers were used to identify the pH dependence of the zeta potential on injection-molded Zeonor® 1060R resin (Fig. 3). The observed pH dependence is sigmoidal and consistent with titration of charged sites with pK_a near 4.8, and is similar in that sense to the pH dependence observed for silica and a number of polymers (*e.g.,*

PMMA, PC). However, the p*I* observed for this polymer is near pH 5, which is significantly higher than that observed for most microfluidic substrate materials. Four different buffers were used to characterize the zeta potential in Fig. 2, and three of these buffers were used to measure the zeta potential in the 8.3–9.3 range. The results are similar (within ± 6% of mean) for these three buffers, indicating that the choice of buffer ion does not significantly affect the observed zeta potential.

3.4 Fabrication technique and specific resin

The measurements presented in Figs. 2 and 3 on injection-molded Zeonor® 1060R are in dramatic contrast to those reported in [8], in which the electroosmotic mobility of hot-embossed Zeonor® 1020R was observed to be zero without a plasma oxidation treatment. To identify whether the fabrication technique or specific resin influence the observed zeta potential, experiments were also performed with devices hot-embossed at Sandia from Zeonor® 1060R and 1020R blanks (blanks were injection-molded at Zeon Chemicals). At the experimental condition tested (pH 7, 10 mM phosphate), insignificant variation was observed between observed zeta potentials (mean ± SD: injection-molded 1060R: − 34 ± 3 mV; hot embossed 1060R: − 32 ± 3 mV; hot-embossed 1020R: − 29 ± 3 mV). The discrepancy between the results presented here and the results presented in [8] is to date unresolved.

3.5 Aging and surface treatments

The effects of incubation and storage on the cyclo-olefin polymers with several different environments were explored. Changes in surface charge with storage conditions affect the applicability of polymer systems, and can be used to infer the chemical nature of the surface charge. All measurements were made at a standard condition (pH 7 phosphate buffer, 10 mM). Storage in air and acetonitrile do not change the measured zeta potential by measurable amounts (Fig. 3). Storage for 10 days in phosphate buffers of varying pHs does lead to a slight increase in the observed zeta potential, and this effect is most dramatic at low pH. These results are also in contrast to the results of [8] in that the electroosmotic mobility of solutions in contact with their plasma-oxidized polymer surfaces were shown to decay over a period of days. The effect of acidic attack on the polymer substrates was measured by exposing the microchannels to perchloric acid and remeasuring the zeta potential. After treatment with perchloric acid, the observed ζ was reduced by approximately one order of magnitude (Fig. 4). For comparison we report in the same graph ζ values from [8].

3.6 Cellulose ethers

Measurements of zeta potential in the presence of hydroxypropylmethylcellulose (HPMC) were used to identify its effect on the apparent zeta potential in Zeo-
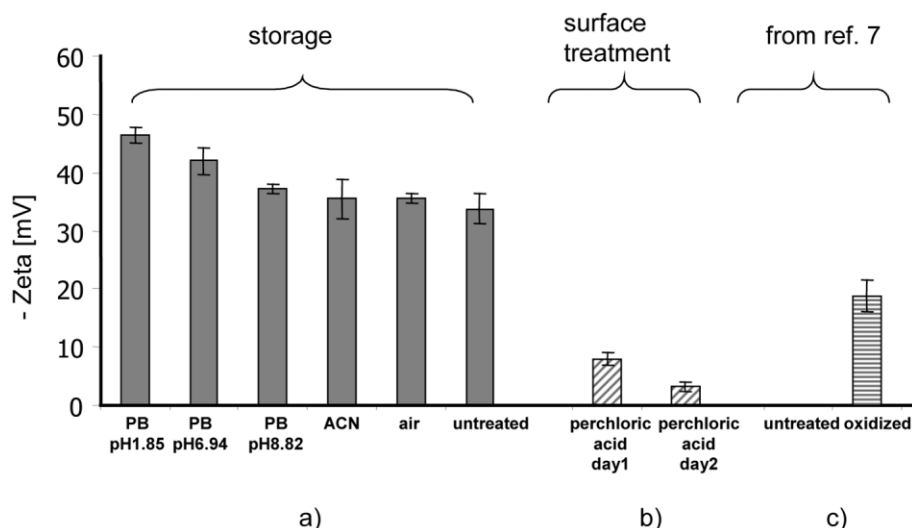

Figure 4. Effect of storage and surface treatment on zeta potential. Abscissa indicates (a) condition in which channels were incubated for one week; (b) effect of 30 min perchloric acid incubation, measured on two sequential days; (c) results for untreated and plasma-oxidized substrates as reported by [8]. Zeta potentials (mean ± SD, n_m = 9, n_c = 3) for (a), (b) were obtained with 10 mM phosphate buffer, pH 7. The data from [8] was measured at 20 mM phosphate pH 7, however, assuming dζ/dlog*C* ≈ 10 mV at pH 7, the difference caused by concentration differences is insignificant as compared to experimental error.

nor®. HPMC is an additive commonly used in capillary electrophoresis to suppress EOF [15–18]. The apparent zeta potential for phosphate buffers with 0.5% w/v HPMC is shown in Table 1 in comparison to the results with buffer alone. In the presence of additives, it is most accurate to report an "apparent" zeta potential that results from calculating the zeta potential using Eq. (1) with the measured bulk viscosity and permittivity (for 0.5% w/v HPMC, μ = 4.0 mPa). The apparent zeta potential thus phenomenologically incorporates any non-Newtonian viscosity effects or spatially varying permittivity changes that may be present in the double layer. ζ is greatly reduced in the presence of HPMC throughout the pH range 1.9–8.8; for pH 6.9 and 8.8, zero is within the 90% confidence interval of the observed values (Table 1).

Table 1. Effect of HPMC on zeta potential at different pH

	Mean ζ (mV) $\pm$ SD		
	pH 1.9	pH 6.9	pH 8.8
Phosphate	46 $\pm$ 3	$-$ 34 $\pm$ 3	$-$ 45 $\pm$ 2
0.5% w/v HPMC in phosphate	12 $\pm$ 2	$-$ 2 $\pm$ 1	1 $\pm$ 4

3.7 Source of charge on polymer surfaces

While the functional form of the observed electrokinetic potential is consistent with titration of a charged site at pK_a = 4.8, no source for such a charged site is clear. The cyclopentadiene structure that dominates the chemical structure of Zeonor® resins does not have any chemical sites expected to ionize in the conditions studied here, thus wall protonation/deprotonation is not expected to be the source of surface charge. Surfaces incubated with amine-functionalized dyes [3] show no fluorescence, indicating that carboxylic acid groups (from oxidation of the cyclopentadiene structure or the presence of proprietary plasticizers) are not present at the wall at a significant concentration.

Adsorption of ions may be postulated as the source of charge on Zeonor® resins; however, the nature of such adsorption processes, if present, is not clear. Polyolefins are hydrophobic (manufacturer's specified contact angle: 94°; observed contact angle on our substrates (mean $\pm$ SD, n_c = 1, n_m = 6): Zeonor® 1060R 90° $\pm$ 2°; Zeonor® 1020R 89° $\pm$ 2°). Adsorption of hydroxyl, hydronium, potassium/sodium, or buffer ions at the surface could be postulated as the source of wall charge. This mechanism has been proposed, for example, as the source of the negative electrokinetic potential observed for Teflon [19];

it is generally argued that simple anions more easily lose their hydration shell and adsorb to hydrophobic surfaces than do their simple cation counterparts. In the present data, measurements with several different buffer ions were used, and the measured zeta potential shows no observable dependence on the buffer ion (note in particular the pH 8–9 region), making it unlikely that buffer ions are potential-determining ions.

3.8 Electrodeless dielectrophoretic trapping of polystyrene beads in cyclo-olefin microstructures

Dielectrophoretic trapping of polystyrene beads in insulating post arrays [20–22] was used to demonstrate the use of Zeonor® microfluidic substrates in an application that is directly affected by electroosmotic effects. A fluorescent bead suspension was introduced to the chip through the fluidic manifolds and a DC applied field was supplied to the chip through two platinum pin electrodes connected to a power supply. Bead behavior was characterized as a function of the applied field. At low field strengths, bead electromigration was observed due to electroosmotic and electrophoretic effects, with electroosmosis dominant at these conditions. At high field strengths, beads tend to be trapped in the post array due to repulsion from the high-field-strength regions in between posts (Fig. 5). Images at a variety of field strengths show these negative dielectrophoretic effects becoming prominent at high field, manifested as discrete particle bands (Fig. 6).
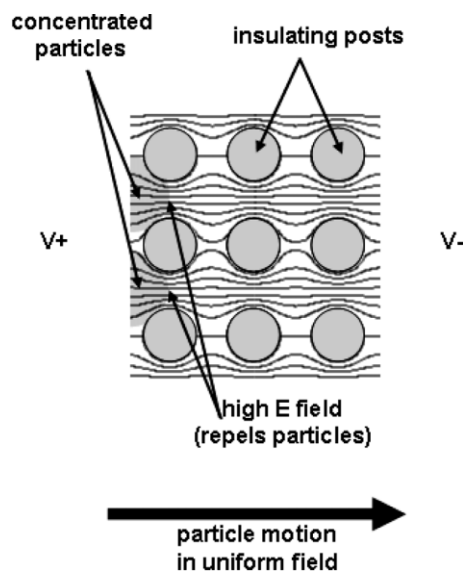

Figure 5. Schematic depiction of the field nonuniformity and attendant particle trapping observed with insulating post arrays.
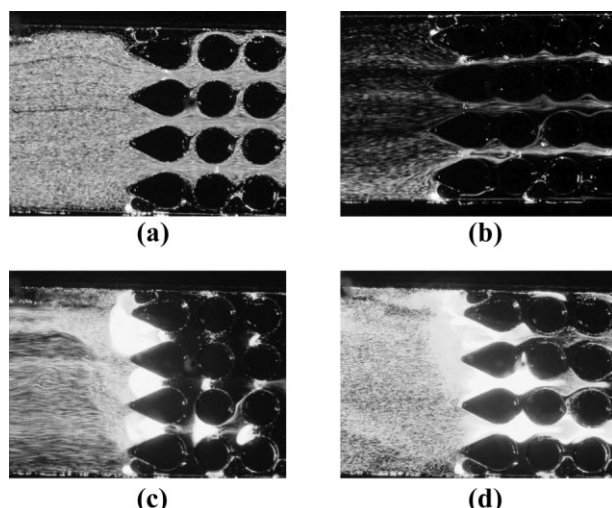
Figure 6. Dielectrophoretic response of fluorescent polystyrene beads in a polymer device constructed entirely of Zeonor® 1060r. (a)–(c): application of bulk fields of (a) 49 V/cm, (b) 392 V/cm, and (c) 980 V/cm. (d) Beads diffuse from the trapping regions when the field is removed. The electroosmotic flow direction is from left to right and is opposite to that of the electric field.

The threshold for complete repulsion of the beads by the high-field-strength region (and therefore macroscopically observed "trapping" in the post array) is given by equality of the net linear electromigratory forces and the nonlinear dielectrophoretic forces. Trapping on Zeonor® is observed at 340 V/cm, as compared to 400 V/cm in glass with similar geometry and fluid conditions [21]. The observed effect is *E*-field addressable, confirmed by the immediate release of beads upon reduction of the *E*-field below the observed threshold and repeatable bead motion upon cycling above and below threshold. The trapping threshold datum (and the observed motion of the negatively charged carboxylate-modified particles in the direction opposite the electric field) both support the observed zeta potentials on the Zeonor® substrates, which are greater in magnitude than those observed for carboxylate-modified latex microspheres (hence motion opposite the *E*-field) but significantly lower than glass (hence reduced linear electromigration and lower trapping threshold). This trapping behavior, demonstrated visually as band widths, is seen to increase until there is virtually no observed bead flow through the post array at 980 V/cm.

4 Concluding remarks

The cyclo-olefin polymer (injection-molded and hot-embossed Zeonor® 1060R and 1020R) microchannels measured in this study exhibit significant zeta potentials

over a wide pH range, in contrast to previous measurements on hot-embossed Zeonor® 1020R channels [8]. Negative zeta potentials at basic conditions and positive zeta potential at acid conditions were observed, consistent with titration of charged sites with $pK_a = 4.8$. Storage in air, acetonitrile, or aqueous solutions at pH 8.8 has a minor effect (10%) on the observed zeta potential. Storage at other pH does have a significant effect ($\sim$ 25–40%). Consistent with observations on hydrophilic surfaces (*e.g.*, oxides), the observed zeta potential was independent of the buffer coion used and varied linearly with the logarithm of the counterion concentration over the range studied (0.5–50 mM). Thus it is likely that buffer co-ions do not adsorb to the surface at significant levels. While the source of the surface charge is unclear, chemical functionalization has shown that carboxylic acid groups are not present at the surface. The apparent zeta potential was drastically reduced when HPMC was added to the running buffer. The same effect was obtained after the channels had been conditioned with 1% solution of perchloric acid. Due to their nonzero surface charge, raw Zeonor surfaces trap polystyrene beads on the anode side of insulating post arrays at lower thresholds than glass substrates.

5 References

[1] Becker, H., Locascio, L. E., *Talanta* 2002, *56*, 267–287.

[2] Johnson, T. J., Ross, D., Gaitan, M., Locascio, L. E., *Anal. Chem.* 2001, *73*, 3656–3661.

[3] Johnson, T. J., Waddell, E. M., Kramer, G. W., Locascio, L. E., *Appl. Surf. Sci.* 2001, *3*, 149–159.

[4] Locascio, L. E., Perso, C. E., Lee, C. S., *J. Chromatogr. A* 1999, *857*, 275–284.

[5] Liu, Y. J., Gauser, D., Scheinder A., Liu, R., Grodzinski, P., Kroutchinina, N., *Anal. Chem.* 2001, *73*, 4196–4201.

[6] Liu, Y. J., Rauch, C. B., Stevens, R. L., Leingk, R., Yang, J., Rhine, D. B., Grodzinski, P., *Anal. Chem.* 2002, *74*, 3063–3070.

[7] Kirby, B. J.,Hasselbrink, Jr., E. F., *Electrophoresis* 2004, *25*, 203–213.

[8] Gaudioso, J., Craighead, H. G., *J. Chromatogr. A* 2002, *971*, 249–253.

[9] Tan, A., Benetton, S., Henion, J. D., *Anal. Chem.* 2003, *75*, 5504–5511.

[10] Kameoka, J., Craighead, H. G., Zhang, H., Henion, J. D., *Anal. Chem.* 2001, *73*, 1935–1941.

[11] Basrour, S., Robert, L., *Mat. Sci. Engineer.* 2000, *288*, 270–274.

[12] Kirby, B. J., Reichmuth, D. J., Renzi, R. F., Shepodd, T. J., Wiedenman, B. J., *Lab Chip* 2005, *5*, 184–190.

[13] Kirby, B. J., Wheeler, A. R., Zare, R. N., Fruetel, J. A., Shepodd, T. J., *Lab Chip* 2003, *3*, 5–10.

[14] Kirby, B. J., Hasselbrink, E. F., *Electrophoresis* 2004, *25*, 187–202.

[15] Buchanan, D. D., Jameson, E. E., Perlette, J., Malike, A., Kennedy, R. T., *Electrophoresis* 2003, *24*, 1375–1382.

[16] Fan, X. J., Liu, J., Tang, H., Jin, Y., Wang, D.-B., *Anal. Biochem.* 2000, *287*, 95–101.

[17] Lindner, H., Helliger, W., Dirschlmayer, A., Jequemar, M., Puschendorf, B., *Biochem. J.* 1992, *283*, 467–471.

[18] Ulvik, A., Refsum, H., Kluijtmans, L. A. J., Ueland, P. M., *Clin. Chem.* 1997, *43*, 267–272.

[19] Lukacs, K. D., Jorgenson, J. W., *J. High Resolut. Chromatogr.* 1985, *8*, 407–411.

[20] Cummings, E. B., Singh, A. K., *Anal. Chem.* 2000, *75*, 4724–4731.

[21] Lapizco-Encinas, B. H., Simmons, B. A., Cummings, E. B., Fintschenko, Y., *Anal. Chem.* 2004, *76*, 1571–1579.

[22] Markx, G., Dyda, P., Pethig, R., *J. Biotechnol.* 1996, *51*, 175–180.